Stellar neutron capture cross sections of the tin isotopes

K. Wisshak,* F. Voss, Ch. Theis, and F. Käppeler
Forschungszentrum Karlsruhe, Institut für Kernphysik, Postfach 3640, D-76021 Karlsruhe, Germany

K. Guber
Oak Ridge National Laboratory, Oak Ridge, Tennessee 37831

L. Kazakov and N. Kornilov
Institute for Physics and Power Engineering, Obninsk, Kaluga Region, Russia

G. Reffo
Comitato Nazionale per la Ricerca e per lo Sviluppo dell'Energia Nucleare e delle Energia Alternative, Centro Dati Nucleari, Via Martiri di Monte Sole 4, I-40138 Bologna, Italy

(Received 19 April 1996)

The neutron capture cross sections of ^{114}Sn, ^{115}Sn, ^{116}Sn, ^{117}Sn, ^{118}Sn, and ^{120}Sn were measured in the energy range from 3 to 225 keV at the Karlsruhe 3.75 MV Van de Graaff accelerator. Neutrons were produced via the ^{7}Li$(p,n)^{7}$Be reaction using a pulsed proton beam. Capture events were registered with the Karlsruhe 4π barium fluoride detector. The experiment was complicated by the small (n,γ) cross sections of the proton magic tin isotopes and by the comparably low enrichment of the rare isotopes ^{114}Sn and ^{115}Sn. Despite significant corrections for capture of scattered neutrons and for isotopic impurities, the high efficiency and the spectroscopic quality of the BaF_2 detector allowed the determination of the cross-section ratios with overall uncertainties of 1–2 %, five times smaller compared to existing data. Based on these results, Maxwellian averaged (n,γ) cross sections were calculated for thermal energies between $kT=10$ and 100 keV. These data are used for a discussion of the solar tin abundance and for an improved determination of the isotopic s- and r-process components. [S0556-2813(96)01509-9]

PACS number(s): 25.40.Lw, 26.20.+f, 27.60.+j, 98.80.Ft

I. INTRODUCTION

The isotopic abundances in the Cd-In-Sn region are characterized by a rather complicated mixture of contributions from various processes of nucleosynthesis [1]. Figure 1 illustrates the two main mechanisms, the slow and rapid neutron capture processes. The reaction flow of the s process follows the sequence of stable isotopes on a time scale of typically a few months, slow compared to average β decays. The dotted arrows indicate the end of the decay chains from the very neutron rich nuclei produced by rapid neutron captures in supernova explosions. Both contributions are difficult to describe due to the numerous isomers in this mass region. A third contribution comes from the p process. During explosive Ne/O burning material is exposed to such high temperatures and densities that photon-induced (γ,n) and (γ,p) reactions can produce the small abundances of the proton rich nuclei [2,3].

Since only even isotopes can survive the hot p-process environment it was suggested that ^{113}In and ^{115}Sn owe their existence to the long-lived isomers indicated in Fig. 1 [4,5]. Though shielded from the main s and r processes, they could be reached by the weak isomeric links at ^{113}Cd and ^{115}In that can be fed by the s-process neutron captures as well as by the r-process β decays.

A detailed study [1] of the branching at ^{113}Cd, based on recent experimental results for the level scheme of this isotope, showed that only 17% of the observed ^{113}In abundance, 6% of ^{114}Sn, and ~50% of ^{115}Sn can be explained by a combined analysis of the s and r processes. To attribute the remaining fraction to the p process is problematic, however, at least for the odd isotopes, which are not produced in due amounts by recent p-process calculations [2,3].

The aim of the present experiment was to improve this situation by an accurate determination of the stellar cross sections of the tin isotopes, an essential prerequisite for detailed s-process analyses. Apart from the puzzling origin of ^{113}In and ^{115}Sn, there is a general interest in an accurate ^{116}Sn cross section. Since this s-only isotope is presumably

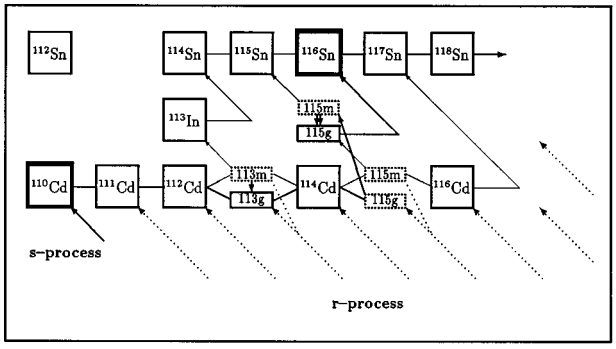

FIG. 1. Possible s- and r-process paths in the Cd-In-Sn region. Only temperature-independent branchings are indicated. (Solid lines, s-process path; dashed lines, post r-process β decays.)

*Author to whom correspondence should be addressed.

not affected by branchings, it could be used for normalizing the $\langle\sigma\rangle N_s$ curve, similar to the previously measured ^{124}Te [6] and ^{150}Sm [7]. In addition, the complete data set allows for a determination of the *s* abundances of all tin isotopes and for an improved separation of the *s*- and *r*-process components in this mass region.

The previous information on the tin cross sections in the keV region originated mainly from a comprehensive study of Timokhov *et al.* [8]. These data were determined for most stable isotopes with typical uncertainties of 5–8 %. In general, the results were found to agree fairly well with older cross sections [9–11], except for ^{120}Sn, where a 20% lower value was reported from an activation experiment [12]. Since all differential data were restricted to the neutron energy range above 20 keV, reliable stellar cross sections could only be calculated for thermal energies larger than $kT=30$ keV, whereas stellar model calculations require these data also around $kT=10$ keV [13,14].

Therefore, it was the aim of the present experiment to extend the investigated neutron energy range from 3 to 225 keV and to reduce the cross section uncertainties to $\sim$1% by using the Karlsruhe 4π BaF_2 detector for registration of capture events. Two complications had to be faced in this work.

(i) The cross sections of the even isotopes are rather small because of the closed proton shell at $Z=50$. In fact, ^{120}Sn exhibits the smallest cross section measured with the Karlsruhe 4π BaF_2 detector up to now. Correspondingly, the unfavorable cross section ratio for neutron scattering and capture gives rise to large corrections for scattered neutrons that are captured in the detector itself.

(ii) Due to the low natural abundances of ^{114}Sn and ^{115}Sn, the available samples were only enriched to 70% and 45% in these isotopes, respectively, resulting in large corrections for isotopic impurities.

While these problems are difficult to handle with conventional time of flight (TOF) methods, the present setup is well suited for treating both corrections properly. This was demonstrated for the more extreme example of the barium isotopes [15], where the background due to capture of scattered neutrons was even larger, and of the gadolinium isotopes [16], where the corrections for isotopic impurities were also larger than in the present case.

The experiment and data analysis are described in Secs. II and III. The differential cross sections are presented in Sec. IV, the uncertainties are discussed in Sec. V, and the determination of the stellar cross sections follows in Sec. VI. The astrophysical implications will be addressed in Sec. VII. A detailed description of the present experiment, including data evaluation methods, calculation of correction factors, and presentation of the results from individual runs, can be found in Ref. [17]. The astrophysical implications have been addressed in Ref. [18].

II. EXPERIMENT

The neutron capture cross sections of the tin isotopes 114–118 and 120 have been measured in the energy range from 3 to 225 keV using gold as a standard. Since the experimental method has been published in detail [6,7,19,20], a brief description will suffice here. Neutrons were produced via the ^{7}Li$(p,n)^7$Be reaction using the pulsed proton beam of the Karlsruhe 3.75-MV Van de Graaff accelerator. The neutron energy was determined by TOF, the samples being located at a flight path of 78.6 cm. Capture events were registered with the Karlsruhe 4π BaF_2 detector via the prompt capture γ-ray cascades. This detector consists of 42 hexagonal and pentagonal crystals forming a spherical BaF_2 shell of 15 cm thickness and 20 cm inner diameter. It is characterized by a resolution in γ-ray energy of 7% at 2.5 MeV, a time resolution of 500 ps, and a peak efficiency of 90% at 1 MeV (for a comprehensive description see Ref. [19]). In the present experiment the γ-ray threshold in the sum energy spectrum could be reduced to 1.6 MeV, resulting in a detection efficiency of $\sim$97% for the even and $\sim$99% for the odd isotopes (see Sec. III).

TABLE I. Sample characteristics.

Sample[a]	Thickness (mm)	Thickness (10^{-3} at/b)[b]	Weight (g)	Neutron binding energy (MeV)
^{116}Sn[c]	2.8	10.2780	7.529	6.944
graphite	1.4	11.9881	0.909	
^{114}Sn	1.0	3.5616	2.589	7.546
^{115}Sn	0.3	1.0303	0.755	9.562
^{197}Au	0.25	1.5048	1.871	6.513
^{117}Sn	0.39	1.2434	0.919	9.326
^{118}Sn	1.8	6.3581	4.737	6.484
empty				
^{120}Sn	3.7	13.5715	10.280	6.171
^{116}Sn[d]	0.90	3.3404	2.447	6.944

[a]All samples are 22 mm in diameter.
[b]For tin samples: sum of all Sn isotopes.
[c]Used in runs 1 and 3.
[d]Used in run 2.

The experiment was divided into three runs, two with the conventional data acquisition technique with the detector operated as a calorimeter and one with the analog-to-digital converter system for obtaining more detailed spectroscopic information. Sample disks of 22 mm diameter were pressed from isotopically enriched metal powder. The relevant parameters of the samples are compiled in Table I. In addition to the six tin samples, a gold sample, a graphite sample, and an empty position in the sample ladder were used in all runs. A second, three times thinner ^{116}Sn sample was prepared in order to check the corrections for neutron multiple scattering and self-shielding effects. The isotopic compositions provided by the supplier are listed in Table II. As already pointed out, the enrichments in ^{114}Sn and ^{115}Sn of 70.2% and 45.3% are comparably low.

The neutron transmissions of the samples are generally larger than 95% except for the thick ^{116}Sn and the ^{120}Sn samples. Normalization of the spectra to equal neutron flux was performed for all samples by means of a ^{6}Li-glass monitor located close to the neutron target. The spectra measured with a second ^{6}Li-glass detector at a flight path of 260 cm were used for a rough determination of the total cross sections. Though the accuracy of this method is inferior to that obtained in a dedicated experiment as performed by Timokhov *et al.* [8], the derived total cross sections can be

TABLE II. Isotopic composition (%).

Sample	Isotope ^{112}Sn	^{114}Sn	^{115}Sn	^{116}Sn	^{117}Sn	^{118}Sn	^{119}Sn	^{120}Sn	^{122}Sn	^{124}Sn
^{114}Sn	0.26	70.2	0.50	10.23	2.40	6.39	1.94	6.68	0.66	0.74
^{115}Sn	0.11	0.57	45.3	33.27	5.21	6.83	1.85	5.68	0.56	0.62
^{116}Sn	<0.03	0.01	0.04	97.6	0.69	0.96	0.16	0.47	0.03	0.04
^{117}Sn	<0.01	<0.01	<0.01	0.84	92.1	5.81	0.39	0.76	0.05	0.05
^{118}Sn	<0.06	<0.03	<0.06	0.07	0.14	98.5	0.78	0.51	<0.04	<0.04
^{120}Sn	<0.01	<0.01	<0.01	0.04	0.03	0.18	0.09	99.6	0.03	0.03

used to test the normalization to equal neutron flux (Sec. III).

The samples were moved cyclically into the measuring position by a computer controlled sample changer. The data acquisition time per sample was about 10 min, a complete cycle lasting about 2 h. From each event, a 64-bit word was recorded on magnetic tape containing the sum energy and TOF information together with 42 bits identifying those detector modules that contributed. During the 78 days of data collection, the overall recorded information was 27 Gbyte.

III. DATA ANALYSIS

A. Total cross sections

The total cross sections of the tin isotopes were determined in the neutron energy range from 10 to 200 keV via the TOF spectra measured with the ^{6}Li glass detector at a flight path of 260 cm. The total cross sections and the related uncertainties were obtained as described in Ref. [7] and are listed in Table III. The values deduced for the carbon sample agree with the data from the joint evaluated file (JEF) [21] within $\pm 3.0\%$, similar to the results reported in Ref. [7]. The uncertainties were again calculated with the assumption that they are inversely proportional to the fraction of neutrons interacting in the sample, $A=1-T$, where T is the transmission. For the carbon sample this fraction was $A=5.4\%$ and an uncertainty of 3% was estimated from the comparison with the JEF data. Correspondingly, the $A=0.9\%$ of the ^{117}Sn sample yields an uncertainty of 18% for the total cross section. For the samples with low enrichment, the uncertainty was attributed to the main isotope after correction for isotopic impurities. Therefore, a 36% uncertainty had to be allowed for the ^{115}Sn sample, where ^{115}Sn contributes only 50% of the total cross section, though it had the same transmission as the ^{117}Sn sample.

The data of Timokhov *et al.* [8], which were obtained in a dedicated experiment using thick samples with transmissions between 60% and 80%, exhibit uncertainties of 0.8–1.4 %. Within the accuracy of the present experiment, there is good agreement for ^{114}Sn, ^{115}Sn, ^{117}Sn, and ^{120}Sn, whereas our results for ^{116}Sn and ^{118}Sn are higher by 12–15 %. This comparison confirms that the present uncertainties were estimated realistically, in particular since the uncertainties of Timokhov *et al.* [8] might have been underestimated for low neutron energies due to the poorer statistics in this part of the spectrum.

The present setup allows one to measure the total cross section with uncertainties between $\sim 2\%$ and $\sim 20\%$ for sample transmissions between 0.92% and 0.99%, respectively. These results provide an independent confirmation of the accuracy obtained in normalizing the spectra of the individual samples to equal neutron flux since they require the uncertainty of this normalization to be less than 0.2%.

B. Capture cross sections

The data analysis was carried out in analogy to the procedure described previously [6,7,20]. All events were sorted into two-dimensional spectra containing 128 sum energy versus 2048 TOF channels according to various event multiplicities (evaluation 1). In evaluation 2, this procedure was

TABLE III. Measured total cross sections (determined from the count rate of the ^{6}Li glass neutron monitor at 260 cm flight path).

Neutron energy (keV)	Total cross section (b) ^{114}Sn	^{115}Sn	^{116}Sn	^{117}Sn	^{118}Sn	^{120}Sn	^{12}C	^{197}Au
10–15	7.32	9.19	6.32	9.09	5.78	5.28	5.13	19.4
15–20	6.07	9.00	6.69	6.73	5.47	5.58	4.64	13.5
20–30	7.26	10.2	6.59	7.08	5.72	5.69	4.93	14.1
30–40	7.54	9.06	7.23	7.93	6.13	5.31	4.90	14.3
40–60	6.55	8.74	6.71	6.55	5.70	5.58	4.70	12.2
60–80	6.92	7.61	6.90	7.18	6.23	6.01	4.58	11.1
80–100	7.07	8.19	6.68	7.56	6.43	5.86	4.59	10.5
100–150	7.39	12.2	7.21	7.47	6.46	6.17	4.38	10.8
150–200	6.70	8.08	6.13	6.79	6.94	6.83	4.14	9.6
Uncertainty	9.2%	36%	2.6%	18%	4.2%	2.1%	3.0%	8.5%

repeated by rejecting those events, where only neighboring detector modules contributed to the sum energy signal. With this option, background from the natural radioactivity of the BaF_2 crystals and from scattered neutrons can be reduced. The spectra of all samples were normalized to equal neutron flux using the count rate of the ^{6}Li-glass monitor near the target.

In further steps of data analysis sample-independent backgrounds were removed and corrections for isotopic impurities and capture of sample scattered neutrons applied. Since experimental data existed only for the six investigated isotopes, the missing TOF spectra of ^{112}Sn and ^{119}Sn were approximated by the spectra of ^{114}Sn and ^{117}Sn, respectively, whereas the ^{120}Sn spectrum was used to mimic the effect of ^{122,124}Sn according to the very similar binding energies of the corresponding isotopes. The abundances of these four impurity isotopes were scaled by factors of 1.54, 0.63, 0.92, and 0.44, in order to account for the proper cross section ratios, which were adopted from the work of Timokhov *et al.* [8]. This simplified treatment was justified by the small abundances of these impurity isotopes, which were always less than 2% (for details see Refs. [7] and [17]).

The resulting corrections for isotopic impurities were much smaller than for the gadolinium isotopes [16], where up to 50% of the measured events had to be subtracted. In the present analysis, the largest corrections of about 20% were required for ^{114}Sn and ^{115}Sn, while they were less than 2% for all other isotopes.

The large ratios of total and capture cross sections of the tin isotopes gave rise to significant corrections for capture of sample scattered neutrons, which were determined in the same way as described previously [7]. For the even tin isotopes, this correction could be evaluated without problems. For the ^{115}Sn and ^{117}Sn, however, the binding energies of 9.5 and 9.3 MeV were larger than those of the odd barium isotopes of the scintillator. Therefore, true capture events were obscured in the γ-ray spectrum by capture events due to scattered neutrons. Accordingly, the scattering correction had to be normalized via the weaker signature of the even barium isotopes as described in Ref. [6], resulting in a correspondingly larger uncertainty. This is particularly critical for ^{115}Sn where the low sample mass and the comparably large correction for isotopic impurities give rise to a reduced statistical accuracy. In turn, this limitation made it difficult to determine the scattering correction for the ^{115}Sn below 10 keV neutron energy.

The resulting corrections for scattered neutrons are included in the TOF spectra of Fig. 2. Compared to the corresponding spectra for the barium isotopes [22], the signal to background ratio is significantly better in the present case, although the capture cross section of ^{120}Sn is almost two times smaller than those of ^{136}Ba and ^{137}Ba. This background reduction illustrates the advantage of the metallic tin samples over the carbonate that had to be used in the barium experiment. At 10 keV neutron energy, for example, the signal to background ratio for ^{120}Sn is better by factors of 5 and 10 compared to ^{136}Ba and ^{137}Ba, respectively.

Figure 2 shows that individual resonances could be resolved up to 20 keV neutron energy in the spectra of ^{116}Sn, ^{118}Sn, and ^{120}Sn. The corresponding resonance parameters will also be extracted from this part of the spectra by a shape analysis program. But whether the stellar cross sections are determined simply by averaging the observed yield or by using the resonance parameters should be of minor importance, similar to the example of ^{136}Ba [23].

After subtraction of the background from scattered neutrons, the TOF spectra of Fig. 2 were used to determine the cross-section shape. For normalization, the two-dimensional data were projected onto the sum energy axis using the TOF region of optimum signal to background ratio as indicated in Fig. 2 by dashed boxes. The resulting pulse height spectrum of the ^{116}Sn sample is shown in Fig. 3. The threshold in sum energy could be lowered to 1.6 MeV by replacing the crystals with the highest radium impurities. The corresponding spectra for the other samples can be found in Ref. [17].

In Fig. 4 the sum energy spectra of ^{120}Sn are shown for different multiplicities of the capture γ-ray cascade according to the number of detector modules contributing per event. The true multiplicities are slightly smaller than these experimental values because of cross talking effects. In the even isotopes, 25–40 % of the capture events are observed with multiplicities $\geqslant 5$, while this fraction is about 60% in the odd isotopes. The arrows in Fig. 4 indicate the range of sum energy channels that were integrated to obtain the TOF spectra of Fig. 2 for determining the cross-section shape. The observed multiplicities exhibit a systematic trend as the neutron number approaches the shell closure at $N=82$. For the even isotopes, the fraction of capture events with multiplicity one increases from 4.8% to 5.3%, and 10.3%, reaching a remarkable extreme of 14% for ^{120}Sn [17].

The cross section ratio of isotope X relative to the gold standard is given by

$$\frac{\sigma_i(X)}{\sigma_i(\mathrm{Au})}=\frac{Z_i(X)}{Z_i(\mathrm{Au})}\,\frac{\Sigma Z(\mathrm{Au})}{\Sigma Z(X)}\,\frac{\Sigma E(X)}{\Sigma E(\mathrm{Au})}\,\frac{m(\mathrm{Au})}{m(X)}F_1F_2. \quad (1)$$

In this expression, Z_i is the count rate in channel i of the TOF spectrum, ΣZ is the TOF rate integrated over the interval used for normalization (Fig. 2), ΣE is the total count rate in the sum energy spectrum for all multiplicities summed over the normalization interval (Fig. 3), and m is the sample thickness in atoms/b. The factor $F_1=[100-f(\mathrm{Au})]/[100-f(X)]$ corrects for the fraction of capture events f below the experimental threshold in sum energy, where X refers to the respective tin sample (Table IV) and F_2 is the ratio of the multiple scattering and self-shielding corrections (Table V).

The fraction of unobserved capture events f and the correction factor F_1 were calculated as described in detail in Ref. [20]. The required input for this calculation are the individual neutron capture cascades and their relative contributions to the total capture cross section as well as the detector efficiency for monoenergetic γ rays in the energy range up to 10 MeV. Capture cascades and capture γ-ray spectra of the involved isotopes were calculated according to the statistical and optical models [24] as in the previous measurements with the 4π BaF_2 detector [6,7,22]. The calculations are based on the Hauser-Feshbach approach. In contrast to the barium experiment [22], where the fraction of cascades with multiplicity 1 was well reproduced, the calculated values for the even tin isotopes are lower by a factor of 2 compared to the experimental results. This indicates either a strong

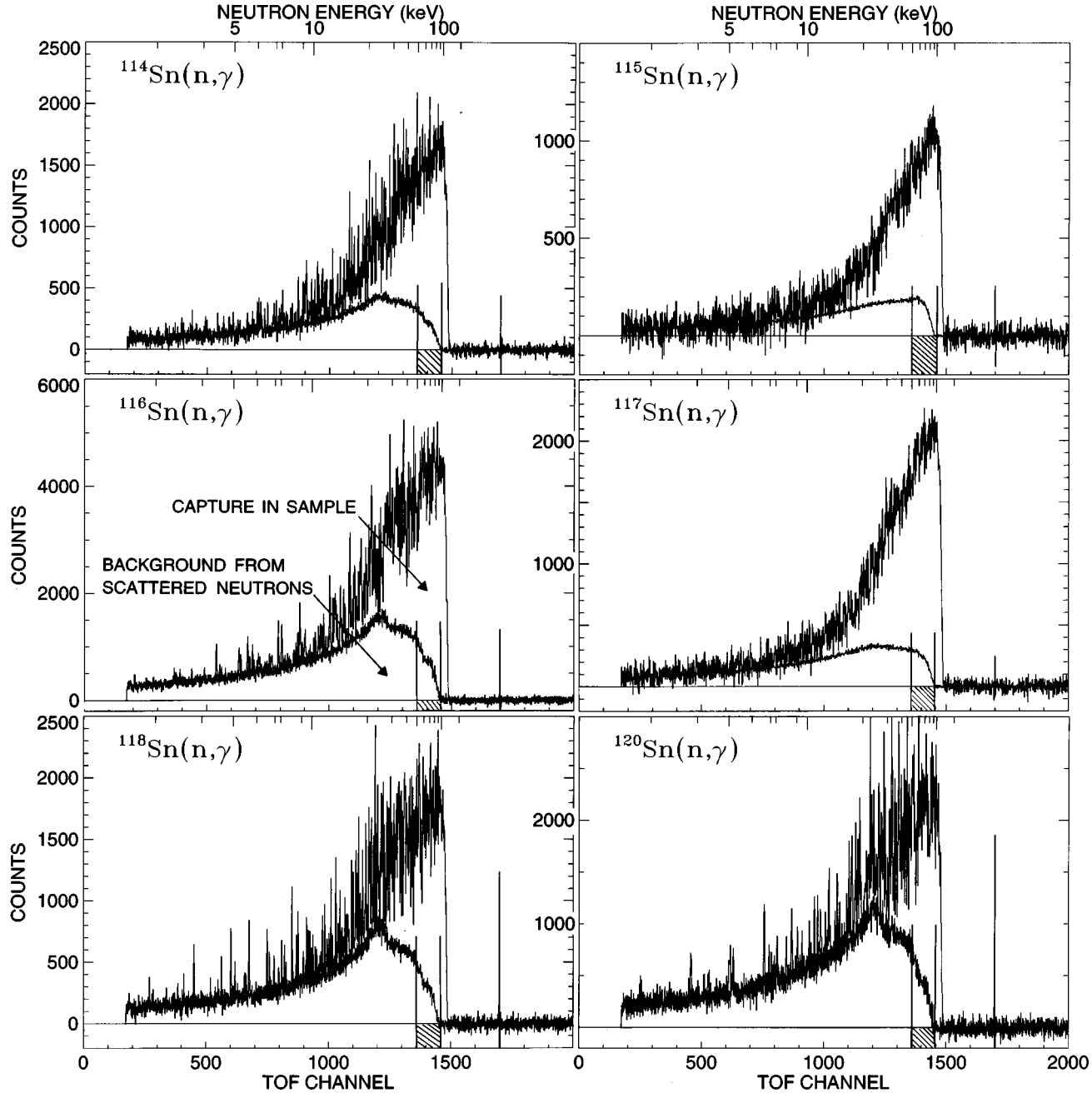

FIG. 2. TOF spectra measured with the tin samples in run 3 with 100 keV maximum neutron energy. The background due to sample scattered neutrons is shown separately. The region used for the absolute normalization of the cross section is indicated by hatched boxes.

nuclear structure effect or a significant contribution from the direct capture channel. Details of the calculations are given in Ref. [17].

The efficiency of the 4π BaF_2 detector was determined experimentally [25] by measuring the response for monoenergetic γ rays produced by (p,γ) reactions on thin ^{26}Mg, ^{30}Si, and ^{34}S targets. In these reactions, certain proton resonances decay predominantly by cascades with only two transitions. By replacing one of the BaF_2 modules with a Ge detector, two-dimensional coincidence spectra, E_γ(Ge) versus $E_\gamma(BaF_2)$, were recorded. The response of the 4π BaF_2 detector for monoenergetic γ rays was then obtained by selecting those events, where the full energy of the complementary γ ray is registered in the germanium detector. With seven (p,γ) resonances and an ^{88}Y source, the line shapes of 20 γ transitions in the energy range from 0.843 to 8.392 MeV could be determined. These data were used in the calculation of the spectrum fractions f and of the correction factors F_1 given in Table IV.

It is important to note that the lower threshold of 1.6 MeV resulted in a significantly improved detector efficiency. While in previous measurements [7,22] the fraction of unobserved capture events for the even isotopes was typically 6–7 %, values of 2–4 % could now be reached.

The correction for neutron multiple scattering and self-shielding was calculated with the SESH code [26]. Apart from

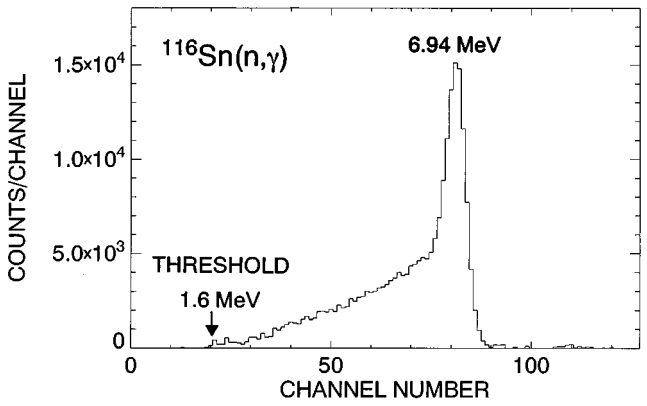

FIG. 3. Sum energy spectrum of ^{116}Sn measured in run 2 containing events with multiplicity greater than 2. This spectrum was obtained by projection of the two-dimensional spectra in the TOF region below the maximum neutron energy indicated by hatched boxes in Fig. 2.

the pairing energies [27], most of the required input parameters were adopted from the work of Timokhov *et al.* [8]. The resulting correction factors F_2 are compiled in Table V. When this code was transferred to a different computer, it turned out that the SESH results depend slightly on the set of random numbers used. Therefore, the multiple-scattering corrections were obtained as the average of eight independent runs and were found to differ by $\sim$1% from the values reported earlier [17]. Since most of this difference refers to the gold sample, the cross-section ratios of the tin isotopes are only marginally affected. This holds for the previous measurements on Te, Ba, Sm, and Gd isotopes as well [6,7,15,16].

The low enrichment of the ^{114}Sn and ^{115}Sn samples implies a possible influence of the isotopic impurities on these corrections. Since most samples of the present experiment are very similar in weight and in size, however, it could be assumed that subtraction of the isotopic impurities via the

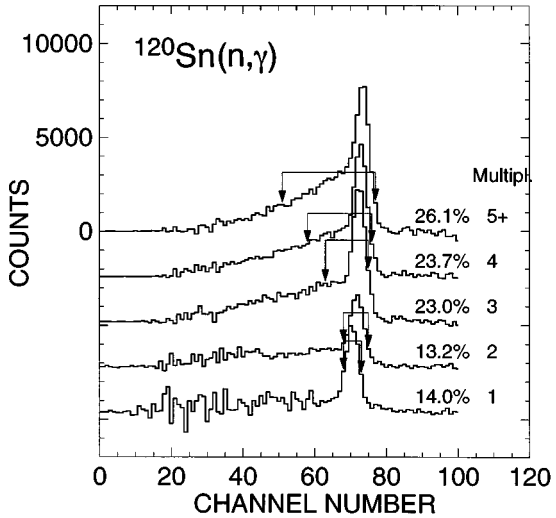

FIG. 4. Sum energy spectra of ^{120}Sn for different detector multiplicities. The regions used for determining the cross section shape are indicated by arrows.

TABLE IV. Fraction of undetected capture events f (%) and the related correction factors F_1 (solid angle 94%, γ-ray threshold 50 keV).

	Threshold in sum energy (MeV)		
	1.5	1.6	2.0
f(Au)	3.56		5.28
$f(^{114}\mathrm{Sn})$	2.06		3.28
$f(^{115}\mathrm{Sn})$	1.27		1.72
$f(^{116}\mathrm{Sn})$	2.52		4.16
$f(^{117}\mathrm{Sn})$	1.14		1.59
$f(^{118}\mathrm{Sn})$	3.56		6.22
$f(^{120}\mathrm{Sn})$	3.76		6.16
$F_1(^{114}\mathrm{Sn/Au})$	0.985	0.984	0.979
$F_1(^{115}\mathrm{Sn/Au})$	0.977	0.974	0.964
$F_1(^{116}\mathrm{Sn/Au})$	0.989	0.989	0.988
$F_1(^{117}\mathrm{Sn/Au})$	0.976	0.973	0.963
$F_1(^{118}\mathrm{Sn/Au})$	1.000	1.002	1.010
$F_1(^{120}\mathrm{Sn/Au})$	1.002	1.003	1.009

spectra of the other samples accounts for the respective contributions to the multiple-scattering corrections as well. Therefore, these corrections were not determined for the true composition of the samples but were calculated as if the two samples consisted of the main isotopes ^{114}Sn or ^{115}Sn only. As shown in Table V, these corrections are below 2% for ^{114,115,117}Sn, the thin ^{116}Sn sample, and for the gold sample, but can be sizable for the other samples as well as at energies below 10 keV. The calculated correction factors can be checked via the results obtained for the two ^{116}Sn samples, in particular below 20 keV, where the differences are large enough to produce a significant effect on the observed count rates (see Sec. V).

IV. RESULTS FOR THE NEUTRON CAPTURE CROSS SECTIONS

The ratios of the neutron capture cross sections of the tin isotopes and of ^{197}Au obtained in the individual runs and via the two evaluation methods discussed above are listed together with the respective statistical uncertainties in Ref. [17]. These data sets do not exhibit systematic effects either for the two evaluation methods or for the various experimental runs where different neutron spectra and different data acquisition modes were used. Only for ^{117}Sn, a systematic difference of $\pm$1.2% was found between evaluations 1 and 2. Though this difference is still within the 2σ limit of the statistical uncertainties, it occurred in all three runs and may be due to the background problems with sample scattered neutrons discussed above.

As in previous measurements with the 4π BaF_2 detector [6,7,22], the final cross section ratios were adopted from evaluation 2. The mean values of the three runs are listed in Table VI together with the statistical, systematic, and total uncertainties. The final uncertainties of the cross section ratios are $\sim$1% for the even and $\sim$2% for the odd isotopes, about five times smaller compared to previous data [8–10,12].

The experimental ratios were converted into cross sec-

TABLE V. Correction factors for the cross section ratios $F_2 = MS(\mathrm{Au})/MS(X)$.

Neutron energy range (keV)	F_2						
	^{114}Sn/Au	^{115}Sn/Au	^{116}Sn/Au [a]		^{117}Sn/Au	^{118}Sn/Au	^{120}Sn/Au
3–5	1.051	1.005	1.215	1.076	1.004	1.166	1.404
5–7.5	1.043	1.015	1.159	1.062	1.012	1.129	1.315
7.5–10	1.039	1.022	1.130	1.052	1.018	1.108	1.265
10–12.5	1.036	1.025	1.112	1.048	1.021	1.096	1.234
12.5–15	1.034	1.026	1.100	1.044	1.022	1.085	1.209
15–20	1.032	1.027	1.086	1.038	1.023	1.075	1.180
20–25	1.031	1.028	1.076	1.035	1.024	1.066	1.154
25–30	1.029	1.028	1.066	1.033	1.023	1.060	1.135
30–40	1.027	1.026	1.056	1.030	1.022	1.051	1.113
40–50	1.024	1.025	1.046	1.026	1.021	1.043	1.095
50–60	1.021	1.024	1.038	1.023	1.020	1.037	1.079
60–80	1.019	1.023	1.030	1.020	1.019	1.030	1.063
80–100	1.016	1.021	1.021	1.016	1.017	1.023	1.047
100–120	1.014	1.020	1.015	1.013	1.016	1.018	1.036
120–150	1.010	1.017	1.007	1.009	1.013	1.012	1.024
150–175	1.008	1.016	1.002	1.006	1.012	1.007	1.015
175–200	1.006	1.015	0.998	1.004	1.011	1.004	1.010
200–225	1.005	1.015	0.995	1.003	1.010	1.001	1.005
Uncertainty (%)	0.5	0.3	0.5	0.5	0.4	0.5	0.7

[a]Thick sample left column, thin sample right column.

tions using the gold cross section of Macklin [28] after normalization by a factor of 0.989 to the absolute value of Ratynski and Käppeler [29] (Table VII). The uncertainties of these data can be obtained by adding the 1.5% uncertainty of the reference cross section to the uncertainties of the respective cross-section ratios.

Compared to the data of Timokhov *et al.* [8], which are quoted with uncertainties of 5–10 % for ^{114,115,116,117}Sn and of 10–20 % for ^{118,120}Sn, the present results are systematically lower by 12%, on average, the individual ratios ranging from 0.80 to 1.00. Most of this systematic difference is due to a $\sim$10% smaller gold cross section used by Timokhov *et al.* [8] for converting the experimental cross section ratios to absolute values. Apart from this problem, all remaining differences are well within the quoted uncertainties [30]. The comparison with all other data will be discussed in Sec. VI in connection with the stellar cross sections.

V. DISCUSSION OF UNCERTAINTIES

The determination of statistical and systematic uncertainties in measurements with the 4π BaF_2 detector has been described in Refs. [6,7,20]. Therefore, the following discussion of the various uncertainties (Table VIII) concentrates on the particular aspects of the present experiment.

In the results for the even tin isotopes no systematic differences were observed either in the different runs or with the different acquisition modes and evaluation methods. This suggests that the systematic uncertainties for background subtraction were negligible, similar to the situation with the samarium isotopes [7]. The difficulties of proper background subtraction in the spectra of the odd isotopes were already discussed in Sec. III with the consequence that the evaluation for ^{115}Sn had to be restricted to the energy range above 10 keV. In case of ^{117}Sn, a systematic difference of $\pm$1.2% between the results of evaluations 1 and 2 can be attributed to background uncertainties in the reference interval used for cross-section normalization. Since part of this difference is due to counting statistics, the systematic part of this normalization uncertainty was assumed to be $\pm$1.0% (see Table VIII). In view of the similar background situation, this uncertainty was considered for ^{115}Sn as well, though no such differences were found for this isotope. The 0.2% uncertainty in neutron flux normalization for the different samples could be verified via the measured total cross sections as discussed in Sec. III A.

The isotopic composition was specified by the supplier with an absolute uncertainty of $\pm$0.2%. Though this seems to be a conservative estimate according to the very good agreement obtained in the independent measurements of the isotopic composition of the samarium samples [7], it was adopted for all isotopes in each sample. This means that the main isotopes in the highly enriched samples are defined with relative uncertainties of 0.2% , but that the low enrichment of the ^{114}Sn and ^{115}Sn samples resulted in correspondingly larger uncertainties of 0.3% and 0.4% (Table VIII).

With the adopted 0.2 % abundance uncertainty, the even (25.2%) and odd (4.8%) impurity isotopes in the ^{114}Sn sample (Table II) yield isotopic corrections with relative uncertainties of 2.0% and 7.2%, respectively. These uncertainties are comparably large since the uncertainties of the various impurity isotopes have to be added in quadrature, resulting in systematic uncertainties of 0.6% for the ^{114}Sn and ^{115}Sn samples.

As noted before, the samples with low enrichment are also problematic with respect to the correction for multiple scattering and self-shielding. The multiple-scattering effect

TABLE VI. Final neutron capture cross-section ratios of ^{114}Sn, ^{115}Sn, ^{116}Sn, ^{117}Sn, ^{118}Sn, and ^{120}Sn relative to ^{197}Au. The abbreviations for uncertainty are denoted as follows: stat, statistical; sys, systematic; and tot, total.

Energy[a]	$\frac{\sigma(^{114}\text{Sn})}{\sigma(^{197}\text{Au})}$	Uncertainty (%)			$\frac{\sigma(^{115}\text{Sn})}{\sigma(^{197}\text{Au})}$	Uncertainty (%)			$\frac{\sigma(^{116}\text{Sn})}{\sigma(^{197}\text{Au})}$	Uncertainty (%)		
(keV)		Stat	Sys	Tot		Stat	Sys	Tot		Stat	Sys	Tot
3–5	0.1619	12.2	1.0	12.2					0.0904	8.4	0.8	8.4
5–7.5	0.1690	6.5	1.0	6.6					0.1700	2.9	0.8	3.0
7.5–10	0.2595	3.7	1.0	3.8					0.1387	3.0	0.8	3.1
10–12.5	0.2566	2.9	1.0	3.1	0.4811	8.8	1.5	8.9	0.1467	2.2	0.8	2.3
12.5–15	0.2030	3.2	1.0	3.4	0.5129	7.0	1.5	7.2	0.1785	1.8	0.8	2.0
15–20	0.2787	1.5	1.0	1.8	0.6143	3.4	1.5	3.7	0.1871	1.1	0.8	1.4
20–25	0.3032	1.2	1.0	1.6	0.7041	2.4	1.5	2.8	0.1820	1.0	0.8	1.3
25–30	0.2165	1.2	1.0	1.6	0.6339	2.0	1.5	2.5	0.1901	0.8	0.8	1.1
30–40	0.2608	0.8	1.0	1.3	0.7207	1.3	1.5	2.0	0.1688	0.6	0.8	1.0
40–50	0.2485	0.8	1.0	1.3	0.7118	1.3	1.5	2.0	0.1547	0.6	0.8	1.0
50–60	0.2339	0.8	1.0	1.3	0.6636	1.3	1.5	2.0	0.1627	0.6	0.8	1.0
60–80	0.2210	0.7	1.0	1.2	0.6191	1.1	1.5	1.9	0.1538	0.5	0.8	0.9
80–100	0.2224	0.7	1.0	1.2	0.6381	1.1	1.5	1.9	0.1519	0.5	0.8	0.9
100–120	0.2143	0.8	1.0	1.3	0.6172	1.2	1.5	2.0	0.1522	0.6	0.8	1.0
120–150	0.2155	1.1	1.0	1.5	0.5635	1.9	1.5	2.4	0.1527	1.1	0.8	1.4
150–175	0.2152	1.2	1.0	1.6	0.5705	2.0	1.5	2.5	0.1582	1.1	0.8	1.4
175–200	0.2270	1.2	1.0	1.6	0.5909	2.1	1.5	2.6	0.1596	1.2	0.8	1.4
200–225	0.2279	1.8	1.0	2.1	0.5827	3.2	1.5	3.5	0.1701	1.7	0.8	1.9

Energy[a]	$\frac{\sigma(^{117}\text{Sn})}{\sigma(^{197}\text{Au})}$	Uncertainty (%)			$\frac{\sigma(^{118}\text{Sn})}{\sigma(^{197}\text{Au})}$	Uncertainty (%)			$\frac{\sigma(^{120}\text{Sn})}{\sigma(^{197}\text{Au})}$	Uncertainty (%)		
(keV)		Stat	Sys	Tot		Stat	Sys	Tot		Stat	Sys	Tot
3–5	0.3556	12.9	1.4	13.0	0.0959	8.8	0.7	8.8	0.0499	14.7	0.9	14.7
5–7.5	0.3447	8.4	1.4	8.5	0.0911	5.3	0.7	5.3	0.0786	5.2	0.9	5.3
7.5–10	0.5144	4.8	1.4	5.0	0.1440	3.1	0.7	3.2	0.0607	5.9	0.9	6.0
10–12.5	0.4987	3.6	1.4	3.9	0.1126	2.9	0.7	3.0	0.0752	3.5	0.9	3.6
12.5–15	0.5428	2.9	1.4	3.2	0.1100	2.7	0.7	2.8	0.0653	3.6	0.9	3.7
15–20	0.5826	1.6	1.4	2.1	0.1170	1.6	0.7	1.7	0.0802	1.8	0.9	2.0
20–25	0.7023	1.1	1.4	1.8	0.1269	1.3	0.7	1.5	0.0705	1.7	0.9	1.9
25–30	0.6512	0.9	1.4	1.7	0.1093	1.1	0.7	1.3	0.0612	1.5	0.9	1.7
30–40	0.6350	0.7	1.4	1.6	0.1120	0.8	0.7	1.1	0.0562	1.2	0.9	1.5
40–50	0.6054	0.7	1.4	1.6	0.0985	0.9	0.7	1.1	0.0570	1.1	0.9	1.4
50–60	0.6078	0.7	1.4	1.6	0.1064	0.8	0.7	1.1	0.0658	1.0	0.9	1.3
60–80	0.5492	0.6	1.4	1.5	0.1032	0.7	0.7	1.0	0.0621	0.9	0.9	1.3
80–100	0.5475	0.6	1.4	1.5	0.1028	0.7	0.7	1.0	0.0618	0.9	0.9	1.3
100–120	0.5219	0.7	1.4	1.6	0.1029	0.8	0.7	1.1	0.0617	1.0	0.9	1.3
120–150	0.5108	1.0	1.4	1.7	0.1053	1.0	0.7	1.2	0.0601	1.4	0.9	1.7
150–175	0.4892	1.1	1.4	1.8	0.1065	1.0	0.7	1.2	0.0667	1.4	0.9	1.7
175–200	0.4149	1.3	1.4	1.9	0.1154	1.1	0.7	1.3	0.0654	1.4	0.9	1.7
200–225	0.3916	2.0	1.4	2.4	0.1146	1.6	0.7	1.7	0.0614	2.0	0.9	2.2

[a]Neutron energy intervals as used for calculating the Maxwellian averaged cross sections.

may be either not completely considered or even overcompensated by subtracting the normalized spectra of the impurity isotopes, in particular if the samples of the impurity isotopes are significantly different in mass. Therefore, the calculation of the correction factors MS were performed for the total sample as well as for the isotope remaining after the isotopic correction. The respective differences were 0.5% and 0.4% for the ^{114}Sn and ^{115}Sn samples, nearly independent of the neutron energy. Analogously to the procedure adopted in the gadolinium experiment [16], 25% of this difference was adopted as an additional systematic uncertainty for these isotopes. For the other isotopes, only the uncertainties provided by the SESH code [26] were considered. This was justified by the reliable set of input data, which allowed one to reproduce the total and capture cross sections consistently.

Eventually, the correction factors for neutron multiple scattering and self-shielding, F_2, were checked via the cross

TABLE VII. Neutron capture cross sections of ^{114}Sn, ^{115}Sn, ^{116}Sn, ^{117}Sn, ^{118}Sn, and ^{120}Sn.

Energy interval [a] (keV)	$\sigma(^{197}\mathrm{Au})$ [b] (mb)	$\sigma(^{114}\mathrm{Sn})$ (mb)	$\sigma(^{115}\mathrm{Sn})$ (mb)	$\sigma(^{116}\mathrm{Sn})$ (mb)	$\sigma(^{117}\mathrm{Sn})$ (mb)	$\sigma(^{118}\mathrm{Sn})$ (mb)	$\sigma(^{120}\mathrm{Sn})$ (mb)
3–5	2266.7	367.1		205.0	806.0	217.5	113.1
5–7.5	1726.7	291.8		293.5	595.2	157.4	135.6
7.5–10	1215.7	315.5		168.7	625.4	175.1	73.8
10–12.5	1066.7	273.7	513.2	156.5	532.0	120.1	80.2
12.5–15	878.0	178.2	450.3	156.7	476.6	96.6	57.4
15–20	738.8	205.9	453.8	138.2	430.4	86.4	59.3
20–25	600.0	181.9	422.5	109.2	421.4	76.1	42.3
25–30	570.8	123.6	361.9	108.5	371.8	62.4	34.9
30–40	500.4	130.5	360.6	84.5	317.8	56.1	28.1
40–50	433.3	107.7	308.4	67.1	262.3	42.7	24.7
50–60	389.6	91.1	258.6	63.4	236.8	41.5	25.7
60–80	349.4	77.2	216.3	53.7	191.9	36.1	21.7
80–100	298.3	66.3	190.4	45.3	163.3	30.7	18.4
100–120	290.1	62.2	179.1	44.1	151.4	29.9	17.9
120–150	274.1	59.1	154.5	41.9	140.0	28.9	16.5
150–175	263.7	56.7	150.4	41.7	129.0	28.1	17.6
175–200	252.6	57.3	149.2	40.3	104.8	29.2	16.5
200–225	248.5	56.6	144.8	42.3	97.3	28.5	15.3

[a]As used for calculating the Maxwellian averaged cross sections.
[b]Based on the ^{197}Au data from the literature [28,29].

sections obtained with the thick and thin ^{116}Sn samples. In the energy intervals from 30 to 80 keV and from 5 to 10 keV these data agree within $\pm 0.2\%$ and $\pm 1.0\%$, while the respective correction factors F_2 differ by as much as 1.3% and 8.4%. Hence this good agreement confirms the reliability of the calculated corrections, especially as the remaining cross-section differences are completely accounted for by the statistical uncertainties.

TABLE VIII. Systematic uncertainties (%). i in ^{i}Sn stands for mass numbers 116, 117, 118, and 120.

Background subtraction in normalization interval	
cross section ratio ^{115,117}Sn/Au	1.0
Flight path	0.1
Neutron flux normalization	0.2
Sample mass (elemental impurities)	0.2
Isotopic composition (^{114}Sn/^{115}Sn/^{i}Sn samples)	0.3/0.4/0.2
Isotopic correction (^{114}Sn/^{115}Sn/^{i}Sn samples)	0.6/0.6/0.2
Multiple scattering and self-shielding: F_2	
cross section ratio ^{114,116,118}Sn/Au	0.5
cross section ratio ^{115}Sn/Au	0.3
cross section ratio ^{117}Sn/Au	0.4
cross section ratio ^{120}Sn/Au	0.7
Undetected events: F_1	
cross section ratio ^{114,116,118,120}Sn/Au	0.4
cross section ratio ^{115,117}Sn/Au	0.8
Total systematic uncertainties	
$\sigma(^{114}\mathrm{Sn})/\sigma(\mathrm{Au})$	1.0
$\sigma(^{115}\mathrm{Sn})/\sigma(\mathrm{Au})$	1.5
$\sigma(^{116}\mathrm{Sn})/\sigma(\mathrm{Au})$	0.8
$\sigma(^{117}\mathrm{Sn})/\sigma(\mathrm{Au})$	1.4
$\sigma(^{118}\mathrm{Sn})/\sigma(\mathrm{Au})$	0.7
$\sigma(^{120}\mathrm{Sn})/\sigma(\mathrm{Au})$	0.9

A detailed discussion of the systematic uncertainties due to undetected events was presented in Ref. [16], where uncertainties of 0.3% for the even and 0.8% for the odd isotopes were estimated for the correction factors F_1 on the basis of two independent sets of calculated capture cascades, in good agreement with the uncertainties quoted in previous measurements with the 4π BaF_2 detector [6,7,22]. Accordingly, the same uncertainties were also adopted in the present case.

VI. MAXWELLIAN AVERAGED CROSS SECTIONS

Maxwellian averaged cross sections were calculated in the same way as described in Refs. [6,20] by dividing the neutron energy range from 0 to 700 keV into three intervals I_x according to the origin of the adopted cross sections. The contributions I_1 from the energy range from 0 to 3 keV were determined in two different ways. First, the cross-section shapes from statistical model calculations were fitted to the present results and at lower energies to the data that were calculated from resonance parameters [31]. In a second calculation, the cross sections of the joint evaluated file [21] were normalized to the present data between 5 and 20 keV, the respective normalization factors ranging from 0.5 to 1.7. In the case of ^{115}Sn, the extrapolation was made for the interval 0–10 keV since no data could be obtained below 10 keV in the present experiment. The uncertainties of 10–15 % assumed for this energy interval correspond to the

TABLE IX. Maxwellian averaged neutron capture cross sections of ^{114}Sn, ^{115}Sn, ^{116}Sn, ^{117}Sn, ^{118}Sn, and ^{120}Sn for thermal energies from 10 to 100 keV (the 1.5% uncertainty of the gold standard is not included here since it cancels out in most applications of relevance for nuclear astrophysics).

kT (keV)	^{114}Sn (mb)	^{115}Sn (mb)	^{116}Sn (mb)	^{117}Sn (mb)	^{118}Sn (mb)	^{120}Sn (mb)
10	249.2±8.4	550.7±42	171.6±2.6	549.4±13	126.6±3.1	73.2±1.7
12	226.2±6.3	512.4±33	155.4±2.1	506.6±10	112.4±2.3	65.1±1.3
20	169.9±3.0	413.2±16	116.1±1.3	395.5±6.5	80.3±1.1	46.7±0.7
25	149.3±2.2	373.2±11	102.1±1.1	351.8±5.5	69.7±0.8	40.5±0.6
30	134.4±1.8	342.4±8.7	91.9±0.9	318.8±4.8	62.6±0.6	36.4±0.5
40	114.6±1.4	298.5±6.3	78.6±0.7	271.4±4.0	53.3±0.6	31.1±0.4
50	102.3±1.2	268.8±5.2	70.5±0.7	239.1±3.5	47.8±0.4	27.9±0.3
52	100.4±1.2	263.9±5.0	69.2±0.6	233.7±3.4	46.9±0.4	27.5±0.3
60	94.1±1.1	247.4±4.5	65.1±0.6	215.0±3.1	44.1±0.4	25.9±0.3
70	88.4±1.1	231.3±4.0	61.2±0.6	196.4±2.8	41.7±0.4	24.5±0.3
80	84.3±1.1	218.5±3.8	58.4±0.6	181.5±2.7	39.9±0.5	23.4±0.4
90	81.0±1.1	208.0±3.4	56.5±0.6	169.3±2.5	38.5±0.5	22.6±0.3
100	78.6±1.3	198.9±3.3	54.7±0.7	159.1±2.6	37.5±0.5	22.0±0.4

observed differences from the mean and include the respective systematic uncertainties. For ^{115}Sn, larger uncertainties of 20% had to be admitted.

The main contributions from the interval I_2 are provided by the cross sections determined in the present experiment (Table VII). The energy grid of these data is sufficiently fine to avoid systematic uncertainties in the averaging procedure.

The energy interval from 225 to 700 keV contributes very little to the Maxwellian average at typical *s*-process temperatures. Up to 460 keV, the experimental cross sections of Timokhov *et al.* [8] were used, complemented by data from the JEF evaluation at higher energies. Both data sets were normalized to the present results in the interval of overlap, assuming that the uncertainties of the normalized cross sections increase from 2% at 225 keV to 10% at 700 keV neutron energy.

A detailed listing of the respective contributions and uncertainties from the intervals I_x is given in Ref. [17]. The resulting Maxwellian averaged cross sections are summarized in Table IX. In most cases, systematic and statistical uncertainties are of the same order. At low thermal energies, however, the statistical uncertainties dominate for all isotopes. The 1.5% uncertainty of the gold standard was not considered in these values since it cancels out in *s*-process studies where cross-section ratios are sufficient.

The present results at $kT=30$ keV are eventually compared in Table X with previous experiments and with the compilations of Bao and Käppeler [32] and Beer, Voss, and Winters [33]. The individual results are in fair agreement, with typical differences of ~10%. A somewhat larger discrepancy of 14% was found for ^{120}Sn. In all cases, the uncertainties have been reduced significantly by the present experimental technique. At this point it was surprising to note the excellent agreement with respect to the oldest measurement: For the even tin isotopes the data of Macklin, Inada, and Gibbons [11] deviate from the present results by only 3.4% on average, despite the fact that a 20% uncertainty had been estimated for these values.

TABLE X. Maxwellian averaged cross sections at $kT=30$ keV compared to previous experiments and evaluations.

	Experiment		Evaluation	
Isotope	Cross section (mb)	Reference	Ref. [32]	Ref. [33]
^{114}Sn	134.4±1.8	present work[a]	184	
	133±7	[8][b]		
^{115}Sn	342.4±8.7	present work[a]	430	
	382±18	[8][b]		
^{116}Sn	91.9±0.9	present work[a]	100±19	92±5
	90±4	[8][b]		
	92±5	[9]		
	104±21	[10]		
	92±19	[11]		
^{117}Sn	318.8±4.8	present work[a]	402±77	402±77
	285±14	[8][b]		
	418±99	[10]		
	390±82	[11]		
^{118}Sn	62.6±0.6	present work[a]	63±12	63±12
	68±4	[8][b]		
	65±13	[10]		
	59±12	[11]		
^{120}Sn	36.4±0.5	present work[a]	39±7	39±7
	31.8±1.2	[12]		
	41.0±3.3	[8][b]		
	41±8	[10]		
	35±7	[11]		

[a]The 1.5% uncertainty of the gold cross section is not included.
[b]Renormalized to gold cross section used in the present work [30].

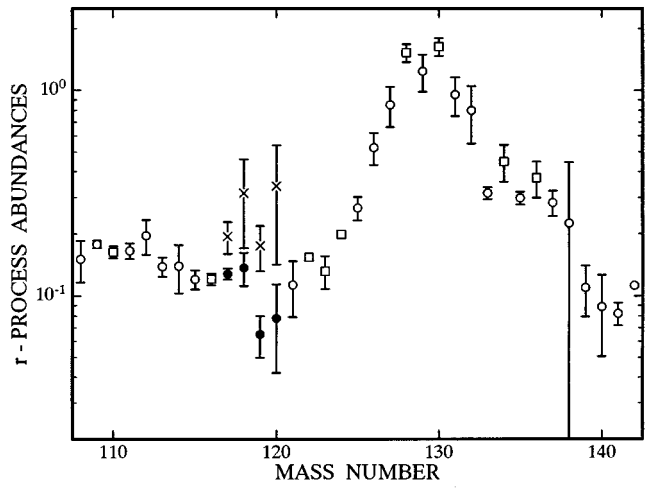

FIG. 5. r-process residuals $N_\odot$-N_s-N_p in the mass region $A=110$–140 for the solar tin abundance of Ref. [35] (crosses) and after normalization to the $\langle\sigma\rangle N$ value of ^{116}Sn (black circles). Pure r nuclei are indicated by squares.

VII. TIN ABUNDANCE AND *R*-PROCESS RESIDUALS

The s-process reaction flow in Fig. 1 exhibits two small branchings at ^{113}Cd and ^{115}Cd that are significant at low temperatures but become negligible above 2.5×10^8 deg when the ground state and isomer in these nuclei are thermally equilibrated [1]. In the classical approach, where the s-process temperature exceeds this value, ^{116}Sn is therefore expected to be one of the unbranched s isotopes that can be used for normalization of the $\langle\sigma\rangle N$ curve via their empirical products of stellar cross section and s abundance.

This argument has been used by Beer *et al.* [9] to suggest a 30% reduction of the meteoritic tin abundance quoted by Anders and Grevesse [34]. With the improved ^{116}Sn cross section it turns out, however, that this empirical value exceeds the meanwhile updated $\langle\sigma\rangle N$ curve only by 15%. While even the reduced ^{116}Sn excess remains far outside the experimental uncertainty, it is almost accounted for by the $\pm10\%$ uncertainty of the solar abundance of this rather volatile element [34,35]. Since the $\langle\sigma\rangle N$ curve is well defined by a number of other s-only isotopes, the ^{116}Sn discrepancy may therefore be ascribed to an overestimated solar tin abundance.

Renormalization of the solar tin abundance to the $\langle\sigma\rangle N$ value of ^{116}Sn has to consider, however, that this isotope carries also a small p-process abundance. If the corresponding contribution of 4% is adopted from the p-process calculations of Howard *et al.* [3,36] and Prantzos *et al.* [2,37], normalization to the $\langle\sigma\rangle N$ curve yields an elemental tin abundance of $N_\odot=3.38$ (Si$=10^6$). This result is lower by 9% and 11%, respectively, compared to the most recent compilations of solar abundances [35,34]. That this normalization is justified can be checked via the abundance pattern of the r-process residuals $N_r=N_\odot-N_s$, which are plotted in Fig. 5. Obviously, this distribution exhibits an irregular pattern if the literature value of the solar tin abundance is used to calculate the r-process residuals (crosses), whereas a smooth distribution in good agreement with the overall trend is obtained via the revised tin abundance (black circles). The decomposition in Table XI is based on the classical approach and assumes a 3% uncertainty for the revised tin abundance to account for the uncertainties of the p-process contribution to ^{116}Sn and of the $\langle\sigma\rangle N$ curve in general. A complete discussion of the intricate s-process reaction flow in the mass region between Cd and Sn and the quest for the origin of the rare isotopes ^{113}In, ^{114}Sn, and ^{115}Sn will be presented in the context of the determination of stellar (n,γ) cross sections of a series of Cd isotopes [18].

TABLE XI. r-process residuals $N_r=N_\odot-N_s-N_p$.

Isotope	N_s [a]	$N_\odot$ [b] $-N_s$	N_p [c]	N_r
^{116}Cd				0.12±0.01
^{116}Sn	0.470±0.005		0.021	
^{117}Sn	0.134±0.002	0.128±0.008		0.128±0.008
^{118}Sn	0.649±0.007	0.164±0.025	0.027	0.137±0.030
^{119}Sn	0.224±0.012	0.065±0.015		0.065±0.015
^{120}Sn	1.005±0.014	0.099±0.036	0.021	0.078±0.038
^{122}Sn				0.154±0.005
^{124}Sn				0.199±0.006

[a]Normalized to $(\langle\sigma\rangle N_s)_{^{124}\mathrm{Te}}=36.00$.
[b]Solar tin abundance normalized to the $\langle\sigma\rangle N_s$ curve including a 4% p-process contribution for ^{116}Sn.
[c]Average values from p-process calculations [2,3].

VII. SUMMARY

The Karlsruhe 4π barium fluoride detector has been improved by replacing the six crystals with the highest α background. In this way, the electronic threshold in the γ-ray spectrum could be reduced to 1.6 MeV, resulting in an improved detection efficiency of 97% and 99% for neutron captures in the even and odd Sn isotopes, respectively.

The total cross sections and the (n,γ) cross sections were measured for the stable isotopes ^{114}Sn, ^{115}Sn, ^{116}Sn, ^{117}Sn, ^{118}Sn, and ^{120}Sn. The total cross sections could be determined from 10 to 200 keV with typical uncertainties from 2% to 10%, except for the odd isotopes, where the large transmission of more than 99% resulted in uncertainties of 20–30 %. The neutron capture cross sections were measured from 3 to 225 keV. In this case, reliable corrections for the sizable isotopic impurities of the ^{114}Sn and ^{115}Sn samples could be determined due to the spectroscopic qualities of the BaF_2 detector. Maxwellian averaged (n,γ) cross sections were derived for thermal energies from 10 to 100 keV with typical uncertainties of 1–2 % for the astrophysically relevant cross section ratios, an improvement by factors of 5–10 compared to existing data. In general, the present results agree within $\sim10\%$ with the data from literature, except for the very small ^{120}Sn cross section.

The accurate cross section of the s-only isotope ^{116}Sn confirmed the supposition [12] that the solar tin abundances given in the compilations of Anders and Grevesse [34] and

of Palme and Beer [35] are too large to be consistent with the overall $\langle\sigma\rangle N$ systematics and a smooth r-process pattern. The suggested reduction of the tin abundance by 12% compared to Ref. [35] is still compatible with the estimated 10% uncertainty of this value, but yields a significantly improved r-process pattern. A complete update of the s-process reaction flow in the mass region of Cd-In-Sn and a discussion of the origin of the rare isotopes ^{113}In, ^{114}Sn, and ^{115}Sn are planned to be presented in a forthcoming paper [18].

ACKNOWLEDGMENTS

We would like to thank F.H. Fröhner and B. Krieg for providing us with the JEF data. The continuous support of the Van de Graaff crew, D. Roller, E.-P. Knaetsch, and W. Seith, who ran the accelerator in a most efficient way, is gratefully acknowledged. Finally, we thank G. Rupp for his skill and patience in optimizing the experimental setup.

[1] Zs. Németh, F. Käppeler, Ch. Theis, T. Belgya, and S.W. Yates, Astrophys. J. **426**, 357 (1994).
[2] N. Prantzos, M. Hashimoto, M. Rayet, and M. Arnould, Astron. Astrophys. **238**, 455 (1990).
[3] W. Howard, B. Meyer, and S. Woosley, Astrophys. J. **373**, L5 (1991).
[4] D. Clayton, Astrophys. J. **224**, L93 (1978).
[5] R. Ward and H. Beer, Astrophys. J. Suppl. **103**, 189 (1981).
[6] K. Wisshak, F. Voss, F. Käppeler, and G. Reffo, Phys. Rev. C **45**, 2470 (1992).
[7] K. Wisshak, K. Guber, F. Voss, F. Käppeler, and G. Reffo, Phys. Rev. C **48**, 1401 (1993).
[8] V.M. Timokhov, M.V. Bokhovko, A.G. Isakov, L.E. Kazakov, V.N. Kononov, G.N. Manturov, E.D. Poletaev, and V.G. Pronyaev, Sov. J. Nucl. Phys. **50**, 375 (1989).
[9] H. Beer, G. Walter, and F. Käppeler, Astron. Astrophys. **211**, 245 (1989).
[10] R. Macklin and J. Gibbons, Rev. Mod. Phys. **37**, 166 (1965).
[11] R. Macklin, T. Inada, and J. Gibbons, Nature **194**, 1272 (1962).
[12] F. Käppeler, W. Schanz, K. Wisshak, and G. Reffo, Astrophys. J. **410**, 370 (1993).
[13] F. Käppeler, R. Gallino, M. Busso, G. Picchio, and C. Raiteri, Astrophys. J. **354**, 630 (1990).
[14] O. Straniero, R. Gallino, M. Busso, A. Chieffi, C. Raiteri, M. Limongi, and M. Salaris, Astrophys. J. **440**, L85 (1995).
[15] F. Voss, K. Wisshak, K. Guber, F. Käppeler, and G. Reffo, Phys. Rev. C **50**, 2582 (1994).
[16] K. Wisshak, F. Voss, F. Käppeler, K. Guber, L. Kazakov, N. Kornilov, M. Uhl, and G. Reffo, Phys. Rev. C **52**, 2762 (1995).
[17] K. Wisshak, F. Voss, Ch. Theis, F. Käppeler, K. Guber, L. Kazakov, N. Kornilov, and G. Reffo, Forschungszentrum Karlsruhe Report No. FZKA-5603.
[18] C. Theis, Ph.D. thesis, University of Heidelberg, 1995 (unpublished).
[19] K. Wisshak, K. Guber, F. Käppeler, J. Krisch, H. Müller, G. Rupp, and F. Voss, Nucl. Instrum. Methods Phys. Res. Sect. A **292**, 595 (1990).
[20] K. Wisshak, F. Voss, F. Käppeler, and G. Reffo, Phys. Rev. C **42**, 1731 (1990).
[21] C. Nordborg, H. Gruppelaar, and M. Salvatores, in *Nuclear Data for Science and Technology*, edited by S. Qaim (Springer, Berlin, 1992), p. 782.
[22] F. Voss, K. Wisshak, K. Guber, F. Käppeler, and G. Reffo, Kernforschungszentrum Karlsruhe, Report No. KfK-5253.
[23] F. Voss, K. Wisshak, and F. Käppeler, Phys. Rev. C **52**, 1102 (1995).
[24] G. Reffo, F. Fabbri, K. Wisshak, and F. Käppeler, Nucl. Sci. Eng. **80**, 630 (1982).
[25] N. Weber, Diplom thesis, University of Karlsruhe, 1993.
[26] F. Fröhner, Gulf General Atomic Technical Report No. GA-8380 (unpublished).
[27] A. Gilbert and A. Cameron, Can. J. Phys. **43**, 1446 (1965).
[28] R. Macklin (private communication).
[29] W. Ratynski and F. Käppeler, Phys. Rev. C **37**, 595 (1988).
[30] Z. Bao (private communication).
[31] J. Mughabghab, M. Divadeenam, and N. Holden, in *Neutron Cross Sections* (Academic, New York, 1981), Vol. 1, Pt. A.
[32] Z. Bao and F. Käppeler, At. Data Nucl. Data Tables **36**, 411 (1987).
[33] H. Beer, F. Voss, and R. Winters, Astrophys. J. Suppl. **80**, 403 (1992).
[34] E. Anders and N. Grevesse, Geochim. Cosmochim. Acta **53**, 197 (1989).
[35] H. Palme and H. Beer, in *Astronomy and Astrophysics*, edited by O. Madelung, Landolt-Börnstein, New Series, Group VI, Vol. VI, Pt. 3a (Springer, Berlin, 1993), p. 196.
[36] W. Howard (private communication).
[37] M. Rayet (private communication).